Boundary-layer model to predict chemically reacting flow within heated, high-speed, micro-tubular reactors

Peter J. Weddle[a], Canan Karakaya[a], Huayang Zhu[a], Raghu Sivaramakrishnan[b], Kirill Prozument[b], Robert J. Kee[a,*]

[a]*Department of Mechanical Engineering, Colorado School of Mines, Golden, CO 80401, United States*
[b]*Chemical Sciences and Engineering Division, Argonne National Laboratory, Argonne, Illinois 60439, United States*

Abstract

Chen-nozzle experiments are used to study the early-stage unimolecular decomposition of larger molecules and, sometimes, the following chemistry. The nozzle itself is typically a small-diameter (order millimeter), short (order 20–50 mm), heated (order 1700 K) tube (nozzle) that exhausts into a vacuum chamber where a variety of diagnostics may be used to measure gas-phase composition. Under typical operating conditions, the velocities are high and the exhaust flow is near sonic. Quantitatively interpreting the measurements requires a model for flow within the nozzle that is coupled with reaction kinetics simulations. The present model shows that the flow can produce significant radial and axial variations in both the thermodynamics conditions and species concentrations. Thus, plug-flow models may not be appropriate. Results show that using He as a carrier gas produces much more plug-like flow than is the case with Ar as the carrier gas. The boundary-layer model provides a computationally efficient approach to modeling detailed chemical kinetics within Chen nozzles. Results are illustrated using acetaldehyde decomposition kinetics.

Keywords: Micro-tubular reactors, Chen nozzle, Boundary-layer model, CANTERA, Acetaldehyde decomposition

1. Introduction

The Chen nozzle was originally developed [1, 2] as a facile, inexpensive, robust, and "clean" source for the generation of highly reactive intermediates (radicals, biradicals, and carbenes). These reactive species are produced at high temperatures under very short contact times in miniature Silicon Carbide (SiC) micro-tubular reactors. In recent years, this Chen nozzle radical source has been used to interrogate complex high temperature dissociation processes in biomass surrogates [3, 4], and PAH/soot precursor formation [5]. There has been an emphasis on using these microreactors to make high temperature kinetics measurements. This has prompted computational fluid dynamics [6] and experimental [7] studies of the complex flow fields within these microreactors.

Figure 1 illustrates aspects of a Chen-nozzle-based experiment to measure chemical kinetics behavior for very-fast high-temperature reactions. The Chen nozzle itself is a short (order 20-50 mm), small diameter (order 1 mm), heated (order 2000 K) tube, through which highly diluted, reactive mixtures flow at high speed. The typical residence times within the tube (Chen nozzle) are from tens to hundreds of microseconds. Upon leaving the tube under choked conditions, the gases rapidly expand to vacuum, which "freezes" the chemistry. A variety of innovative diagnostics may be used to interrogate the flow and composition of reactive and non-reactive gas mixtures [8].

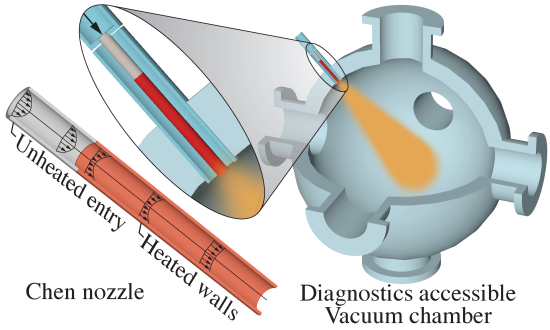

Figure 1: Central aspects of an experiment based on the Chen nozzle.

Quantitative interpretation of the measurements depends upon a model of the reaction chemistry within the nozzle. The simplest models simply solve the ho-

*Corresponding author: Tel: (303) 273-3379
Email address: rjkee@mines.edu (Robert J. Kee)

mogeneous mass-action kinetics problem as a function of time (e.g., Sivaramakrishnan, et al. [9]). Other models are based on plug-flow assumptions (e.g., Zhang, et al., [10]). The plug-flow models allow the specification of axial temperature profiles and predict axial pressure variations. However, both the plug-flow and mass-action models necessarily neglect any radial variations within the tubes. A recent study by Guan, et al., [6], which developed a model based on the full Navier–Stokes equations, showed that radial variations can be significant. However, the computational cost of solving the Navier–Stokes equations makes the inclusion of detailed chemistry impractical. The present approach, based on the axisymmetric boundary-layer equations, enables the inclusion of detailed chemistry and retains all the essential characteristics of the full Navier–Stokes model. Even with large chemical kinetics mechanisms, the boundary-layer models can be solved on a typical personal computer in a few minutes.

Although the flow rates are high, a dimensional analysis shows that because the nozzle diameter is small the Reynolds numbers are on the order of Re $\approx$ 1000. Thus, the flow remains laminar. Further scaling analysis shows that the "boundary-layer" approximations are appropriate, meaning that axial diffusive transport is negligible. This leads to very significant simplifications of the full Navier–Stokes equations, yet retains the full axisymmetric flow field [11, 12]. Consequently, a high-fidelity and computationally efficient model can be developed to assist the quantitative interpretation of Chen nozzle experiments.

2. Model attributes and advances

The Navier–Stokes models make clear that velocity and temperature vary axially and radially and the pressure variation is dominantly axial [6]. Thus, it is clear that the chemistry must have significant axial and radial variations. Consequently, models based on plug-flow assumptions (i.e., neglecting radial variation) significantly compromise chemical predictions, and hence quantitative interpretation of Chen-nozzle experiments. The boundary-layer formulation retains the essential axisymmetric flow characteristics, yet permit the practical incorporation of detailed chemical kinetics.

Chemically reacting boundary-layer models were first reported by Coltrin, et al., [13, 14] for applications in chemical vapor deposition. Broadly speaking, the model formulation and computational approaches are well documented [11, 12]. To date, these models have been applied to low-speed applications. However, to accommodate the high-speed attributes of the Chen nozzle, some additional considerations are relevant. These include

- The gas-phase energy equation needs to include terms that describe irreversible viscous dissipation Φ and retain the often-neglected flow-work contribution, $u\,\partial p/\partial z$).
- Models must accommodate the possibility that the high-speed flow can "choke," meaning that the exit flow cannot exceed the sonic velocity (i.e., Mach one). This requires an iterative adjustment of the inlet pressure to assure that the choked-flow condition is not violated.
- As the pressure decreases and velocity increases (especially near the nozzle exit), the Knudsen number increases. The rarefied flow behavior requires the imposition of partial-accommodation boundary conditions at tube walls.

3. Boundary-layer model summary

As derived in Kee, et al. [11], the steady-state, axisymmetric, chemically reacting, laminar, boundary-layer equations can be expressed in Von Mises coordinates as

$$\rho u\frac{\partial u}{\partial z}+\frac{\partial p}{\partial z}=\rho u\frac{\partial}{\partial \psi}\left(\mu\rho u r^2\frac{\partial u}{\partial \psi}\right), \tag{1}$$

$$0=\frac{\partial r^2}{\partial \psi}-\frac{2}{\rho u}, \tag{2}$$

$$0=\frac{\partial p}{\partial \psi}, \tag{3}$$

$$\rho u\frac{\partial Y_k}{\partial z}=-\rho u\frac{\partial\left(r j_{k,r}\right)}{\partial \psi}+\dot{\omega}_k W_k, \tag{4}$$

$$\begin{aligned}\rho c_p u\frac{\partial T}{\partial z}&=u\frac{\partial p}{\partial z}+\rho u\frac{\partial}{\partial \psi}\left(\lambda\rho u r^2\frac{\partial T}{\partial \psi}\right)\\&\quad-\sum_{k=1}^{K}c_{\mathrm{p},k}j_{k,r}\left(\rho u r\frac{\partial T}{\partial \psi}\right)-\sum_{k=1}^{K}h_k\dot{\omega}_k W_k+\Phi.\end{aligned} \tag{5}$$

The independent variables are the axial coordinate z and the stream function ψ. The dependent variables are the axial velocity u, temperature T, pressure p, the mass fractions Y_k, and the radial coordinate r. The density ρ follows from the ideal-gas equation of state. Other variables include the dynamic viscosity μ, species volumetric molar production rates $\dot{\omega}_k$, thermal conductivity λ, molecular weights W_k, species enthalpies h_k, and heat capacities $c_{p,k}$.

The radial species diffusive flux $j_{k,r}$ can be expressed as

$$j_{k,r} = -\rho^2 ur \frac{W_k}{\overline{W}} D'_{km} \left[\frac{\partial X_k}{\partial \psi} + (X_k - Y_k) \frac{1}{p} \frac{\partial p}{\partial \psi} \right], \quad (6)$$

where D'_{km} is the mixture averaged diffusion coefficient for species k, $\overline{W}$ is the mean molecular weight, and X_k is the mole fraction of species k. The viscous dissipation term can be simplified in the boundary-layer setting as

$$\Phi = \mu \left(\rho ur \frac{\partial u}{\partial \psi} \right)^2. \quad (7)$$

3.1. Slip boundary conditions

A significant consideration in the Chen Nozzle experiment is whether the gas dynamics can be explained using continuum mechanics [6]. The boundary-layer equations assume that the flow is in the continuum regime, but under typical operating conditions the flow can become sonic at the exit (i.e., the Mach number is unity). These conditions result in rarefied flow near the exit of the nozzle. Partial accommodation (i.e., slip) boundary conditions are imposed at the nozzle walls. The velocity slip, proposed by Maxwell for curved surfaces, can be expressed as

$$u_s = \frac{2 - \sigma_v}{\sigma_v} \lambda_D \left(-\frac{\partial u}{\partial r} + \frac{\partial v}{\partial z} \right)_{r=R} + \frac{3}{4} \frac{\mu}{\rho T} \frac{\partial T}{\partial z}\bigg|_{r=R}, \quad (8)$$

where u_s is the slip velocity at the wall, σ_v is the tangential momentum accommodation factor, and λ_D is the mean free path of the particles in the flow, and R is the reactor radius [15]. The mean free path can be expressed as

$$\lambda_D = \frac{k_B T}{\sqrt{2} \pi d^2 p}, \quad (9)$$

where d is the molecular diameter. Similarly the temperature jump (or slip) condition as proposed by Smoluchowski can be expressed as

$$T_s - T_{wall} = -4 \frac{2 - \sigma_T}{\sigma_T} \frac{2\gamma}{\gamma + 1} \frac{\lambda_D}{\mu c_p} \lambda \frac{\partial T}{\partial r}\bigg|_{r=R}, \quad (10)$$

where T_s is the temperature of the fluid at the wall, T_{wall} is the wall temperature, σ_T is the energy accommodation coefficient, and γ is the ratio of specific heats (c_p/c_v) [16].

The slip boundary conditions can be transformed to Von Mises coordinates as

$$u_s = -\rho ur \frac{2 - \sigma_v}{\sigma_v} \lambda_D \frac{\partial u}{\partial \psi}\bigg|_{r=R} + \frac{3}{4} \frac{\mu}{\rho T} \frac{\partial T}{\partial z}\bigg|_{r=R}, \quad (11)$$

$$T_s - T_{wall} = -\rho ur \frac{2 - \sigma_T}{\sigma_T} \frac{2\gamma}{\gamma + 1} \frac{\lambda_D}{\mu c_p} \lambda \frac{\partial T}{\partial \psi}\bigg|_{r=R}. \quad (12)$$

The accommodation factors for the partial-slip boundary conditions (Eqs. 11 and 12) are assumed to be $\sigma_v = 0.75$ and $\sigma_T = 0.9$ [17, 18]. The atomic diameters (Eq. 9) are taken to be $d_{Ar} = 3.33$ Å and $d_{He} = 2.576$ Å.

3.2. Choked-flow condition

The model itself does not require that the flow be choked at the exit. However, as Chen-nozzle experiments are typically configured, the nozzle exhausts to a vacuum chamber. Thus, the normal situation is that the flow is choked at the exit. When the flow is choked at the exit, the Mach number must approach unity at the exit. When the mass flow rate is specified (as typically measured via mass flow control), the inlet pressure must vary so as to achieve the sonic exit and maintain the specified flow rate.

The inlet pressure is iteratively adjusted to ensure the flow is choked at the exit. To begin the iteration, reasonable inlet pressures between 0.2 and 0.1 atm are assumed [6, 7]. The model is run simulating only the bath gas to reduce the computation time to the order of seconds. If the flow does not choke, the inlet pressure is reduced. If the flow chokes before the exit, the inlet pressure is increased.

A "choked" flow condition at the exit means that the radially-distributed Mach numbers approach unity. When the choked condition is reached, the independent variables in the boundary-layer equations become asymptotic. This asymptotic relationship as the Mach number reaches unity has been analytically derived in constant cross-section adiabatic flows [19]. The model reports the distance down the reactor where the choked condition is reached. It is reasonable to develop an iterative numerical method to adjust the inlet pressure based on this output, but currently the inlet pressure is adjusted by hand.

3.3. Computational solution

The boundary-layer model is solved using a method-of-lines formulation [11]. Derivatives in the cross-stream dimension (i.e., stream function) are discretized on a non-uniform finite-volume mesh. The axial coordinate is the time-like coordinate. The discretized system forms a differential-algebraic system of equations (DAE), which is solved in MATLAB[1] using the

[1] The MathWorks, Inc; Natick, MA,USA; www.mathworks.com

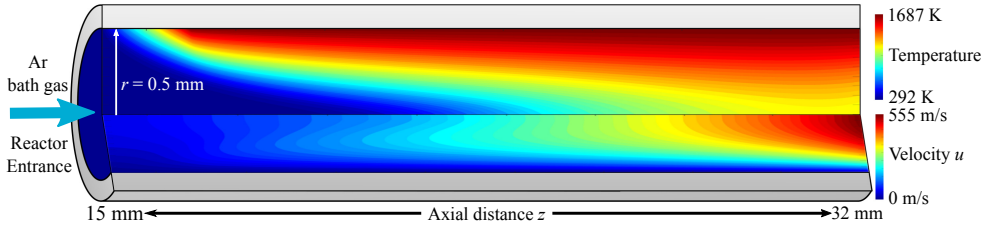

Figure 2: Temperature and velocity contour plots within the heated region of the nozzle. The carrier gas is Ar. Because the tube diameter (1 mm) is so small compared to the length (17 mm), the radial coordinate is greatly expanded for clarity.

Table 1: Boundary-layer model geometry, boundary and initial conditions using argon as a bath gas [6, 9].

Variable	Description	Value
D	Tube diameter	1 mm
L_{ent}	Entrance length	15 mm
L_{ramp}	Ramping length	2 mm
L_{hot}	Reactor length	15 mm
$T_{\text{w,ent}}$	Entrance wall temperature	300 K
T_{hot}	Reactor wall temperature	1700 K
T_{in}	Inlet gas temperature	300 K
p_{in}	Inlet pressure	0.21 atm
$X_{\text{in,Ar}}$	Inlet Ar mole fraction	0.999
$X_{\text{in,CH}_3\text{CHO}}$	Inlet CH_3CHO mole fraction	0.001
$\dot{m}$	Inlet mass flow rate	8.32E-6 kg s^{-1}
$\dot{V}_{\text{in}}$	Inlet volume flow rate	280 sccm

ode15i function. The thermodynamic properties, transport properties and chemical reaction rates are evaluated using the CANTERA software[2].

The results shown in the following section use a reaction mechanism that consists of 34 species and 78 reactions. The cross-stream non-uniform mesh consists of 50 finite volumes. With Ar as the carrier gas, the computation time is approximately 10 minutes on a typical personal computer. With only 15 cross-stream finite volumes the computation time is approximately 1 minute. Computation times are somewhat longer with He as the carrier gas.

4. Results and discussion

To illustrate the model and explore flow characteristics, consider the thermal decomposition mechanism of acetaldehyde (CH_3CHO) as reported by Sivaramakrishnan et al. [9]. Table 1 lists specific nozzle dimensions and operating conditions, which are largely based on the geometry and operating conditions discussed by Guan, et al. [6]. Using a specified inlet volumetric flow rate (here, $\dot{V}_{\text{in}} = 280$ sccm), the inlet pressure p_{in} is adjusted to a achieve near-sonic choked exit.

[2]www.cantera.org

The flow enters an unheated entry region where the wall is maintained at 300 K. Following 15 mm of unheated wall, the wall temperature ramps linearly to 1700 K over a distance of 2 mm. The wall temperature then remains fixed at 1700 K for another 15 mm, whereupon the flow exits the tube to vacuum. It should be noted that the wall temperature profiles are usually more complicated in particular experiments and the model can accommodate any wall-temperature profile. However, for the illustrative purposes here, the relatively simple profile is suitable for characterizing the flow field and its effects on chemistry.

In addition to the reaction mechanism itself and supporting thermodynamic data (Sivaramakrishnan et al. [9]), the boundary-layer model requires transport properties for each participating species. Note that transport data is not needed for homogeneous mass-action models of plug flow models. The reaction mechanism, together with thermodynamic and transport parameters (i.e., Lennard-Jones well depth, collision diameters, ...) are reported in the Supplementary Material.

Figure 2 shows temperature and velocity contour plots for the nominal flow conditions. These results show clearly that strong radial and axial variations persist throughout the flow field. As is easily anticipated, the near-surface fluid heats more rapidly than the interior fluid closer to the centerline.

Figure 3 illustrates the pressure p, axial velocity u, temperature T, and Mach number profiles as functions of axial position at selected radii. The qualitative behavior of the profiles changes significantly upon the flow entering the heated region at approximately 15 mm.

The pressure decrease is primarily the result of viscous drag on the tube walls. Note that a central tenet of the boundary-layer theory is that the radial momentum equation (Eq. 3) reduces neglecting radial pressure gradients [11]. Thus, as indicated by Fig. 3a, the pressure is a function of axial position alone.

The axial-velocity profiles (Fig. 3b) illustrate the expected acceleration of the flow due to heating. The ve-

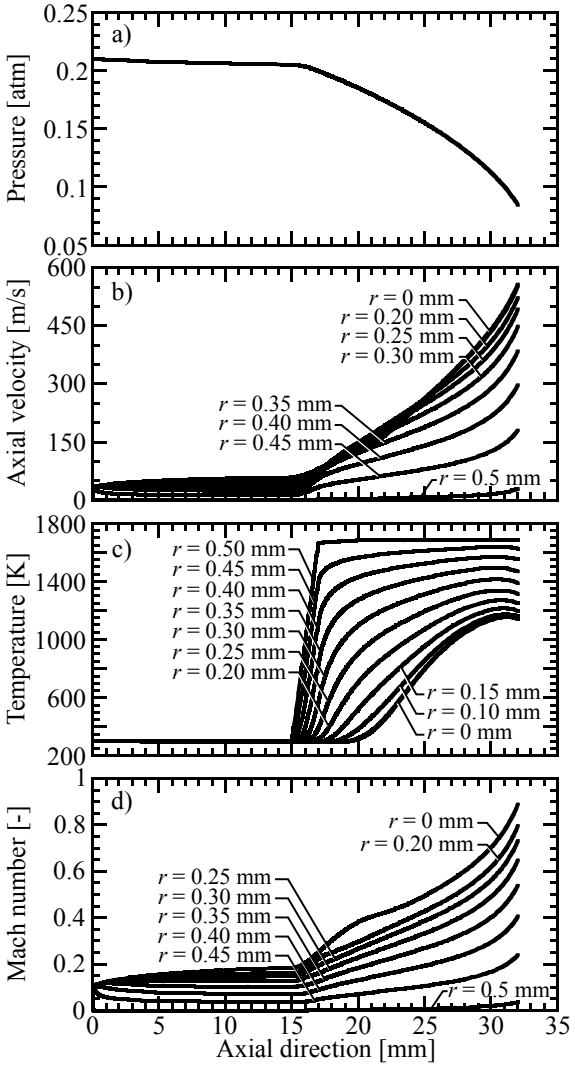

Figure 3: Pressure, axial velocity, temperature, and Mach-number profiles as functions of axial position with argon as a bath gas. Table 1 shows the operating parameters.

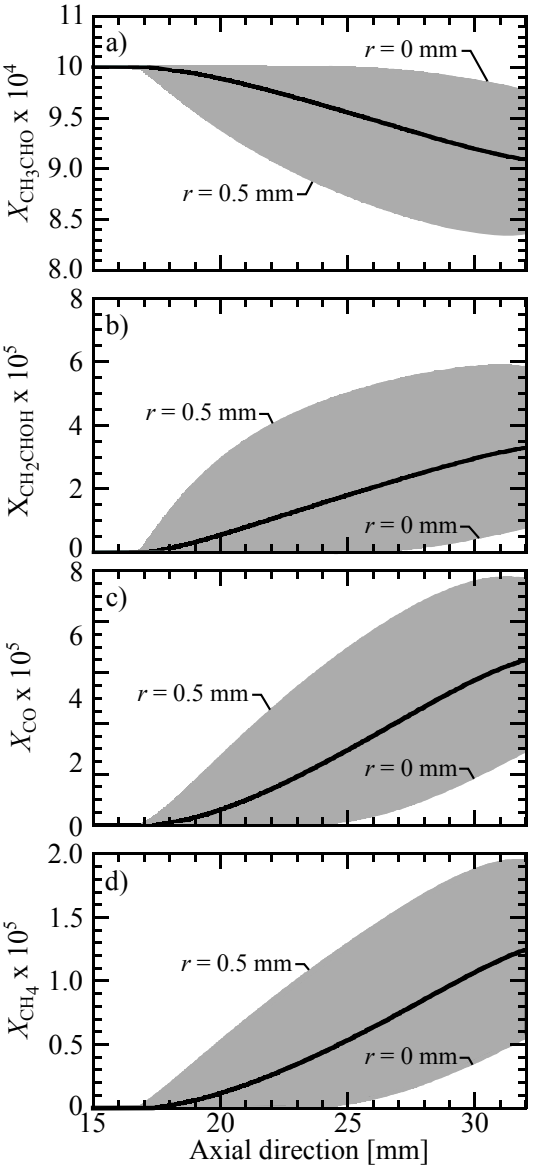

Figure 4: Species mole fraction profiles as a function of axial distance into the reactor with argon as a bath gas. The black lines indicate the radial-mean mole fraction for each species. The gray regions indicate the range of mole fractions radially.

locity gradient in the radial direction is especially significant near the exit where the center-line velocity approaches 560 m s^{-1} and the slip velocity at the nozzle wall is approximately 30 m s^{-1}. The strong radial gradients in the axial velocities cause significant variations in local residence time, which in turn affects the chemistry.

Figure 3c reveals large temperature variations. Because reaction rates typically depend exponentially on temperature, the large temperature variations produce large variations in local chemical reaction rates. Figure 3d shows the Mach number profiles. The Mach number is greatest near the centerline where the velocity is high and the temperature is low.

Recently, these micro-reactors are being extended for use in chemical kinetics studies [6] by measuring species compositions. Thus, predicting and interpreting the species profiles within the nozzle is important. Figure 4 illustrates predicted profiles for selected species mole fractions as a function of axial distance into the reactor. The radially averaged mean mole fractions are illustrated as the black lines. At each axial position, the

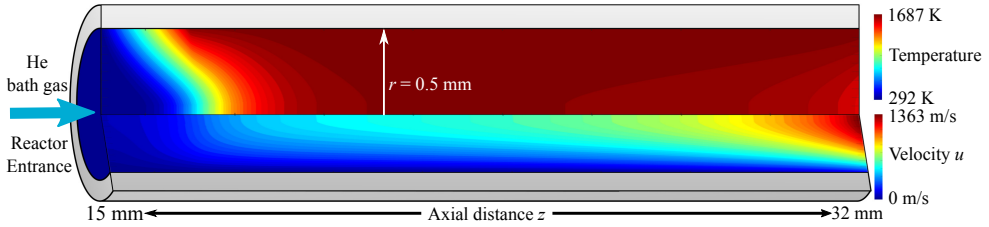

Figure 5: Temperature and velocity contour plots within the heated region of the nozzle. The carrier gas is He. Because the tube diameter (1 mm) is so small compared to the length (17 mm), the radial coordinate is greatly expanded for clarity.

species mass flow rates are evaluated as

$$\dot{m}_k = 2\pi \int_0^{\psi_0} Y_k d\psi, \tag{13}$$

where $\psi_0 = \dot{m}/2\pi$. The mean mass fractions are $\overline{Y}_k = \dot{m}_k/\dot{m}$, with the mean mole fractions following as

$$\overline{X}_k = \frac{\overline{Y}_k/W_k}{\sum_{k=1}^{K} \overline{Y}_k/W_k}. \tag{14}$$

The gray regions indicate the range of mole fractions across the radius. For example, Fig. 4a illustrates CH_3CHO as a function of axial position within the reactor. Because the fluid temperature is highest near the outer radius (i.e., tube wall), the acetaldehyde decomposes most rapidly in the outer radial regions. Additionally, the fluid velocity is slower in the outer radii, which effectively increases the residence time.

The foregoing results are based upon using Ar as the carrier gas. The following results consider He as the carrier gas, which has significantly higher thermal conductivity and lower viscosity. Thus, it may be anticipated that the using He may diminish the radial variations. Consider the situation with operating conditions being generally the same as in Table 1, including the inlet volume flow rate remaining fixed as $\dot{V}_{\text{in}} = 280$ sccm. However, using He, the mass flow rate becomes $\dot{m} = 8.42 \times 10^{-7}$ kg s^{-1} and inlet pressure must be changed to $p_{\text{in}} = 0.16$ atm such that the Mach number at the centerline of the reactor is near unity at the exit and the flow remains choked.

Figure 5 shows contour plots that are comparable to Fig. 2, but with the carrier gas switched to He. With He as the carrier, despite the strong radial variation in the axial velocity, the temperature profile approaches that of a plug flow.

Figure 6 shows that the species profiles also reasonably approximate plug-flow behavior. In other words, the band of species profiles is much more closely grouped around the mean mole fraction profiles. While there are substantial differences in the radial-mean species profiles (and their ranges) with the two bath gases, CH_3CHO decomposition is shown to be initiated to a noticeable extent in both the simulations. The observed products evolve as a result of the numerous unimolecular and bimolecular reactions shown to be active in the prior CH_3CHO theory/modeling work [9]. There are some obvious advantages to using He as the bath gas to establish near-plug-flow like conditions within the Chen nozzle. However, heavier bath gases such as Ar can be used to take advantage of specific diagnostic capabilities (e.g. stronger signals in CP-mm wave spectroscopy due to more effective rotational cooling in the supersonic expansion [8]).

4.1. Discussion on transition to turbulence

Because of the high-speed flow, transition to turbulence may be possible under some conditions. Traditionally transition to turbulence is expected to start when the Reynolds number at the inlet ($\text{Re}_{\text{in}} = \rho_{\text{in}} V_{\text{in}} D/\mu_{\text{in}}$) approaches 1800. The inlet Reynolds numbers for the argon and helium cases discussed in the present paper are $\text{Re}_{\text{in,Ar}} = 459$ and $\text{Re}_{\text{in,He}} = 466$, respectively. These low Reynolds numbers indicate that the inlet flow is laminar. To estimate transition to turbulence as the flow accelerates, a local Reynolds number $\text{Re} = \rho u D/\mu$ may be evaluated throughout the nozzle (radial and axial). The temperature increase and pressure decrease along the length of the nozzle result in specially varying density, velocity, and viscosity. The density decreases with increasing temperature and decreasing pressure, the velocity increases as the flow accelerates toward the sonic exit, and the viscosity increases with temperature. These locally varying properties compete to influence the local Reynolds number. The maximum local Reynolds number for the argon and helium cases are $\text{Re}_{\text{max,Ar}} = 1400$ and $\text{Re}_{\text{max,He}} = 1120$, respectively. Thus, the flow is expected to remain laminar throughout.

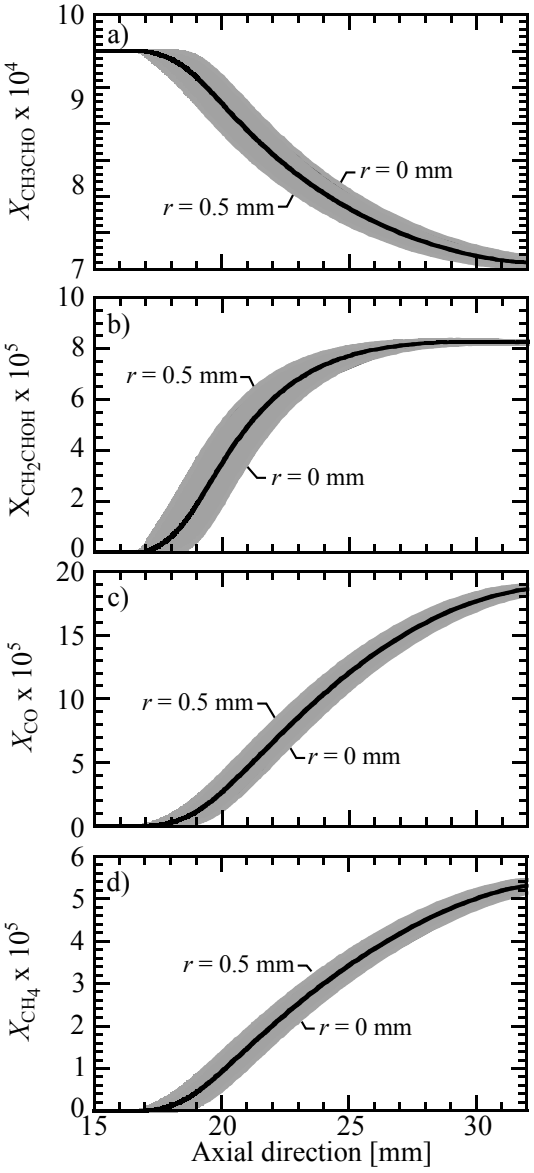

Figure 6: Species mole fraction profiles as a function of axial distance into the reactor with helium as a bath gas. The black lines indicate the radial-mean mole fraction for each species. The gray regions indicate the range of mole fractions radially.

5. Summary and conclusions

A computationally efficient boundary-layer model has been developed to predict chemically reacting flow in a Chen nozzle. The model accommodates attributes of the high speed choked flow that is typical of Chen-nozzle experiments. The fluid mechanical behavior is comparable to that from a full Navier–Stokes model, but the computational times are greatly reduced. Thus, the new model enables the practical incorporation of complex chemical reaction mechanisms. In this way, the model can be used to interpret diagnostics measurements in the context of detailed reaction mechanisms.

Broadly speaking, it is desirable to use relatively simpler plug-flow models to interpret micro-tubular reactor (e.g. Chen-nozzle) experiments. The boundary-layer results show that the actual flow field depends strongly on the fluid properties of the carrier gas. For the conditions considered in the present study, using Ar as a carrier produces a flow field that is far from plug flow. However, using He as the carrier gas produces a flow field that can be reasonably approximated as plug flow. On the other hand, cold pockets may preserve and transport unstable reactive intermediates and thus significantly affect the chemistry. Modeling such flows is important for applications such as combustion and gas-phase biomass decomposition.

The model can be used quantitatively to evaluate and interpret measured data. In this context, it can be of great value in the development of reaction mechanisms. Such a model cannot directly predict reaction pathways and rate parameters. However, the model can be used to evaluate the validity of proposed reaction mechanisms insofar as their ability to predict measured species concentrations. The model can be easily extended to incorporate capabilities such as sensitivity analysis, which many mechanism developers find to be helpful.

The results reported here consider specified wall-temperature profiles. However, the model is implemented to consider the more complex case of an electrically heated SiC tube wall. In this case, the tube wall temperature is determined by solving the coupled thermal balance within the wall, including conductive and radiative transport.

Acknowledgments

This research was supported at CSM by the Office of Naval Research via grant N00014-16-1-2780. The effort at ANL was supported by the U.S. Department of Energy, Office of Science, Office of Basic Energy Sciences, Division of Chemical Sciences, Geosciences, and Biosciences under contract No. DE-AC02-06CH11357. We gratefully acknowledge insightful discussions on compressible high-speed flow with Prof. Greg Jackson (CSM).

References

[1] Kohn, D.; Clauberg, H.; Chen, P. Flash pyrolysis nozzle for generation of radicals in a supersonic jet expansion. *Rev. Sci. Instrum.* **1992**, *63*, 4003.

[2] Blush, J.; Clauberg, H.; Kohn, D.; Minsek, D.; Zhang, X.; Chen, P. Photoionization mass and photoelectron spectroscopy of radicals, carbenes, and biradicals. *Acc. Chem. Res.* **1992**, *25*, 385–392.

[3] Urness, K.; Guan, Q.; Golan, A.; Daily, J.; Nimlos, M.; Stanton, J.; Ahmed, M.; Ellison, G. Pyrolysis of furan in a microreactor. *J. Chem. Phys.* **2013**, *139*, 124305.

[4] Urness, K.; Guan, Q.; Troy, T.; Ahmed, M.; Daily, J.; Ellison, G.; Simmie, J. Pyrolysis pathways of the Furanic Ether 2-Methoxyfuran. *J. Phys. Chem. A* **2015**, *119*, 9962–9977.

[5] Parker, D.; Kaiser, R.; Bandyopadhyay, B.; Kostko, O.; Troy, T.; Ahmed, M. Unexpected chemistry from the reaction of Naphthyl and Acetylene at combustion-like temperature. *Angew. Chem. Int. Ed.* **2015**, *54*, 5421–5424.

[6] Guan, Q.; Urness, K.; Ormand, T.; David, E.; Ellison, G.; Daily, J. The properties of a micro-reactor for the study of the unimolecular decomposition of large molecules. *Intl. Rev. Phys. Chem.* **2014**, *33*, 447–487.

[7] Tranter, R.; Kastengren, A.; Porterfield, J.; Randazzo, J.; Lockhart, J.; Baraban, J.; Ellison, G. Measuring flow profiles in heated miniature reactors with X-ray fluorescence spectroscopy. *Proc. Combust. Inst.* **2017**, *36*, 4603–4610.

[8] Prozument, K.; Park, G.; Shaver, R.; Vasiliou, A.; Oldham, J.; David, D.; Muenter, J.; Stanton, J.; Suits, A.; Ellison, G.; Field, R. Chirped-pulse millimeter-wave spectroscopy for dynamics and kinetics studies of pyrolysis reactions. *Phys. Chem. Chem. Phys.* **2014**, *16*, 15739–15751.

[9] Sivaramakrishnan, R.; Michael, J.; Harding, L.; Klippenstein, S. Resolving some paradoxes in the thermal decomposition mechanism of acetaldehyde. *J. Phys. Chem. A* **2015**, *119*, 7724–7733.

[10] Zhang, Y.; Cai, J.; Zhao, L.; Yang, J.; Jin, H.; Cheng, Z.; Li, Y.; Zhang, L.; Qi, F. An experimental and kinetic modeling study of three butene isomers pyrolysis at low pressure. *Combust. Flame* **2012**, *159*, 905–917.

[11] Kee, R.; Coltrin, M.; Glarborg, P.; Zhu, H. *Chemically Reacting Flow, Theory, Modeling, and Simulation*; Wiley: Hoboken, NJ, 2018.

[12] Raja, L. L.; Kee, R. J.; Deutschmann, O.; Warnatz, J.; Schmidt, L. D. A Critical Evaluation of Navier-Stokes, boundary-layer, and plug-flow Models of the Flow and Chemistry in a Catalytic-Combustion Monolith. *Catal. Today* **2000**, *59*, 47–60.

[13] Coltrin, M.; Kee, R.; Miller, J. A Mathematical Model of the Coupled Fluid Flow and Chemical Kinetics in a Chemical Vapor Deposition Reactor. *J. Electrochem. Soc.* **1984**, *131*, 425–434.

[14] Coltrin, M.; Kee, R.; Miller, J. A Mathematical Model of Silicon Chemical Vapor Deposition: Further Refinements and the Effects of Thermal Diffusion. *J. Electrochem. Soc.* **1986**, *133*, 1206–1213.

[15] Lockerby, D.; Reese, J.; Emerson, D.; Barber, R. Velocity boundary condition at solid walls in rarified gas calculuations. *Phys Rev E* **2004**, *70*.

[16] Smoluchowski, M. Ueber Wärmeleitung in verdünnten Gasen. *Annalen der Physik* **1898**, *300*, 101–130.

[17] Arkilic, E.; Schmidt, R.; Breuer, K. Gaseous slip flow in long microchannels. *J. Microelectromech. Syst.* **1997**, *6*, 167–178.

[18] Ameel, T.; Barron, R.; Wang, X.; Warrington, R. Laminar forced convection in a circular tube with constant heat flux and slip flow. *Microscale Therm. Eng.* **1977**, *4*, 303–320.

[19] Shapiro, A. *The dynamics and thermodynamics of compressible fluid flow*; The Ronald Press Company: New York, NY, 1953; pp 163–170.